British Journal of Pharmacology 172.12 (2015): 3159-76

DOI: 10.111/bph.13117

Toll-like receptor 4 contributes to vascular remodelling and endothelial dysfunction in angiotensin II-induced hypertension

*R Hernanz[1], *S Martínez-Revelles[2], R Palacios[1], A Martín[1], V Cachofeiro[3], A Aguado[2], L García-Redondo[2], M T Barrús[1], P R de Batista[1], A M Briones[2], M Salaices[2] and M J Alonso[1]

*These authors have equally contributed

[1]Dept. of Ciencias Básicas de la Salud, Universidad Rey Juan Carlos, Alcorcón, Spain and Instituto de Investigación Hospital Universitario La Paz (IdiPaz) Madrid, Spain. [2]Dept. of Farmacología, Universidad Autónoma de Madrid and IdiPaz, Madrid, Spain. [3]Dept. of Fisiología, Universidad Complutense de Madrid, Madrid, Spain

Short running title: TLR4 and vascular damage in hypertension

RH, SM-R, RP, AM, VC, AA, LG-R, MTB and PRB performed the research
RH, AMB, MS and MJA, designed the research study
RH, SM-R and AA analysed the data
RH, AMB, MS and MJA, wrote the paper
RH, SM-R, RP, AM, VC, AA, LG-R, MTB, PRB, AMB, MS and MJA approved the MS

Correspondence:
Dr. Mª Jesús Alonso
Departamento de Ciencias Básicas de la Salud
Facultad de Ciencias de la Salud, Universidad Rey Juan Carlos
Avda. de Atenas s/n, 28922 Alcorcón, Spain
Phone: 00-34-91-4888875; Fax: 00-34-91-4888831
e-mail: mariajesus.alonso@urjc.es

Dr. Mercedes Salaices
Departamento de Farmacología y Terapéutica
Facultad de Medicina, Universidad Autónoma de Madrid
Calle Arzobispo Morcillo s/n, 28029 Madrid
Phone: 00-34-91-4975378; Fax: 00-34-91-4975380
e-mail: mercedes.salaices@uam.es

Abstract

BACKGROUND AND PURPOSE

TLR4 signalling contributes to inflammatory cardiovascular diseases, but little is known about its role in hypertension and the associated vascular damage. We investigated whether TLR4 activation contributes to angiotensin II (AngII)-induced hypertension and the associated vascular structural, mechanical and functional alterations.

EXPERIMENTAL APPROACH

We used aorta and mesenteric arteries from mice infused or not with AngII (1.44 $mg \cdot Kg^{-1} \cdot day^{-1}$, 2 weeks, sc) treated with the neutralizing anti-TLR4 antibody or IgG (1 $\mu g \cdot day^{-1}$), and cultured vascular smooth muscle cells (VSMC) from hypertensive rats.

KEY RESULTS

Aortic TLR4 mRNA levels were greater in AngII-infused than control mice. Anti-TLR4 antibody treatment of AngII-infused mice improved: 1) the increased blood pressure and MCP-1, TNFα and IL-6 levels; 2) the vascular structural changes; 3) the increased vascular stiffness, the diminished wall distensibility, the altered elastin structure and the collagen deposition; 4) the altered aortic phenylephrine- and ACh-induced responses; 5) the increased NOX-1 mRNA levels, superoxide anion production and NAD(P)H oxidase activity and the effects of catalase, apocynin, ML-171 and Mito-TEMPO on vascular responses; and 6) the reduced NO release and the L-NAME effect on phenypehrine-induced contraction. In VSMC, the MyD88 inhibitor ST-2825 reduced the AngII-induced NAD(P)H oxidase activity; moreover, the TLR4 inhibitor CLI-095 reduced the AngII-induced increased phospho-JNK1/2 and p65 NF-κB subunit nuclear protein expression.

CONCLUSIONS AND IMPLICATIONS

TLR4 upregulation by AngII contributes to the inflammation, endothelial dysfunction, vascular remodelling and stiffness associated with hypertension by mechanisms probably involving oxidative stress. MyD88-dependent activation and JNK/NF-κB signalling pathways might contribute to these alterations.

Key words: TLR4, hypertension, oxidative stress, vascular remodelling, endothelial dysfunction

List of non-standard abbreviations: AngII, angiotensin II; dAUC, differences of area under the concentration-response curves; DAMPs, damage-associated molecule patterns; ECM, extracellular matrix; HSP, heat shock proteins; IL-6, interleukin-6; IEL, internal elastic lamina; KHS, Krebs-Henseleit solution; L-NAME, N^G-nitro-L-arginine methyl ester; ML-171, 2-acetylphenothiazine; MCP-1, monocyte chemoattractant protein-1; $O_2^{\cdot -}$, superoxide anion; ROS, reactive oxygen species; SHR, spontaneously hypertensive rats; TLR4, Toll-like receptor 4; TNFα, tumor necrosis factor α; VSMC, vascular smooth muscle cells.

Introduction

Structural alterations or vascular remodelling, increased stiffness and endothelial dysfunction are key features of hypertension and are associated to vascular smooth muscle cells (VSMC) reorganization, increased extracellular matrix (ECM) deposition and altered contractility or impaired endothelium-dependent relaxation (Mulvany, 2008; Briones *et al.*, 2010; Rizzoni and Agabiti-Rosei, 2012; Ponticos and Smith, 2014). Both endothelial dysfunction and remodelling of small vessels are relevant prognostic factors of cardiovascular events in high-risk population (de Ciuceis *et al*., 2007; Mathiassen *et al*., 2007; Münzel *et al*., 2008). Therefore, elucidating the mechanisms responsible for these alterations is of enormous interest.

It is recognized that chronic-low grade inflammation has a crucial role in the pathogenesis of hypertension (Savoia and Schiffrin, 2006). The role of adaptive immunity in the pathogenesis of hypertension has been recently reported (for review, see de Ciuceis *et al*., 2014; Harrison, 2014; Schiffrin, 2014). Angiotensin II (AngII) is now considered a proinflammatory mediator in hypertension through mechanisms involving reactive oxygen species (ROS) production that contribute to the observed vascular alterations. (Touyz, 2005; Briones *et al*., 2009; Briones and Touyz, 2010). However, how the inflammation associated with this pathology is initiated has not been fully elucidated. Toll-like receptor 4 (TLR4) is a member of pattern recognition receptors which plays an important role mediating inflammatory response (Carpenter and O´Neill, 2009; McCarthy *et al*., 2014). Besides being expressed in immune cells, TLR4 is ubiquitously expressed in cells of the cardiovascular system and in fact contribution of TLR4 signalling has been proposed in vascular inflammatory pathologies such as atherosclerosis, diabetes or metabolic syndrome (den Dekker *et al*., 2010; Jialal *et al*., 2014). Moreover, we and others have recently described an emerging role for TLR4 in hypertension. Thus, TLR4 expression is increased in hypertension, and this expression seems to be associated with the increased blood pressure (Eiβler *et al*., 2011; Bomfin *et al*., 2012; Marketou *et al*., 2012; Sollinger *et al*., 2014; de Batista *et al*., 2014). TLR4 is activated by lipopolysaccharide as well as by non-infectious host-endogenous compounds (damage-associated molecule patterns, DAMPs), such as heat shock proteins (HSP), fibrinogen and tenascin-C, many of which are present in hypertension as a consequence of chronic cell injury and death (Tsan and Gao, 2004; McCarthy *et al*., 2014). Furthermore, AngII upregulates TLR4 expression that contributes to the proinflammatory effects of this factor (Wolf *et al*., 2006; Ji *et al*., 2009; Yuen *et al*., 2012). In this sense, we have described that through AT1 receptors AngII contributes to the vascular TLR4 upregulation found in spontaneously hypertensive rats (SHR) (de Batista *et al*., 2014). After activation, TLR4 signalling might occur via MyD88 (myeloid differentiation factor 88)-dependent or -independent pathways that ultimately activate NF-κB, which controls transcription of several proinflammatory genes (Carpenter and O´Neill, 2009; Kawai and Akira, 2010).

Recent studies have demonstrated that TLR4 is involved in the vascular dysfunction observed in SHR and N^G-nitro-L-arginine methyl ester (L-NAME)-induced hypertension (Sollinger *et al*., 2014; de Batista *et al*., 2014). While the imbalance between Th1 effector and the anti-inflammatory Treg lymphocytes in the progression of vascular remodelling in hypertension has been proposed (Schiffrin, 2014; de Ciuceis *et al*., 2014; Harrison, 2014), to the best of our knowledge, the involvement of TLR4 in the structural and mechanical alterations observed in this pathology has not still been explored. Therefore, we investigated whether TLR4 contributes to AngII-induced hypertension and the associated vascular structural, mechanical and functional alterations focusing on the role of oxidative stress in these alterations. Our findings

provide novel evidence that TLR4 mediates AngII-induced hypertension and inflammation as well as the vascular functional alterations and remodelling associated to this pathology. Our results also suggest that the JNK/NF-κB signalling pathways and increased oxidative stress from NAD(P)H oxidase and mitochondria may be implicated in these vascular effects through MyD88-dependent activation.

Methods

Animal models

All procedures were approved by the Ethical Committee of Research of the Universidad Autónoma de Madrid, Spain (CEI-UAM 31-759) and are in accordance with the guidelines for ethical care of experimental animals of the European Community, the current Spanish and European laws (RD 223/88 MAPA and 609/86), and the Animal Research: Reporting In Vivo Experiments (ARRIVE) guidelines.

The following C57BL6 male mice were used: 1) control mice treated with a non-specific IgG (IgG_{2a}, 1 μg·day^{-1}, saline-diluted, i.p., Santa Cruz Biotechnology Inc., Dallas, TX, USA); 2) infused with AngII (1.44 mg·Kg^{-1}·day^{-1} for 2 weeks, s.c. by Alzet osmotic minipumps, Alza Corp., Cupertino, CA, USA) and treated with IgG; 3) infused with AngII and treated with the neutralizing anti-TLR4 antibody (rat monoclonal IgG_{2a}, 1 μg·day^{-1} saline-diluted, i.p., Santa Cruz Biotechnology Inc.). For some experiments, control mice treated with anti-TLR4 antibody were also used; treatment did modify neither blood pressure nor structural and mechanical parameters of mesenteric arteries nor aortic vascular responses (results not shown). Treatments started 24 h prior to AngII infusion. Systolic BP was measured by tail-cuff plethysmography. In addition, VSMC obtained from adults SHR were also used.

Tissue preparations

Animals were euthanized by CO_2 and aorta and first order branches of the mesenteric artery were dissected free of fat and connective tissue and maintained in cold (4°C) Krebs-Henseleit solution (KHS, in mM: 115 NaCl, 25 $NaHCO_3$, 4.7 KCl, 1.2 $MgSO_4.7H_2O$, 2.5 $CaCl_2$, 1.2 KH_2PO_4, 11.1 glucose, and 0.01 Na_2EDTA) bubbled with a 95% O_2-5% CO_2 mixture (pH=7.4). The analyses of vascular structure and function as well as NO production were made on the same day. For superoxide anion ($O_2^{\cdot-}$) production measurement, segments were placed in KHS containing 30% sucrose for 20 min, transferred to a cryomold containing Tissue Tek OCT embedding medium and frozen in liquid nitrogen. For immunofluorescence and histological studies, arterial segments were fixed with 4% paraformaldehyde (PFA; in 0.2 M phosphate buffer, pH=7.2-7.4) for 1 h and washed in three changes of PBS. After washing, arterial segments were frozen as described above. Segments used for gene expression studies were immediately frozen in liquid nitrogen. Tissues were kept at -70°C until the day of the experiments. The hearts were removed to assess cardiac hypertrophy. For this, the ratio between the left ventricular wet weight and the length of the tibia was calculated.

Cell culture

Primary cultures of VSMC were obtained from thoracic aortas from 5 months-old SHR using the explant method (Martín *et al*., 2012). Cells were identified as VSMC by morphological and growth characteristics and by positive immunocytochemical staining with a specific monoclonal anti-α-actin antibody (Sigma Chemical Co., St Louis, MO, USA). For experiments, cells from passages 2 to 5 were rendered quiescent by incubation in DMEM containing 0.2% FBS for 24 h. Cells were stimulated with 100 nM AngII (for the times indicated in the results section), with or without pretreatment for 1 h with the MyD88 inhibitor ST-2825 (20 μM) or the TLR4 inhibitor CLI-095 (1 μM).

Pressure myography

The structural and mechanical properties of small mesenteric arteries were studied with a pressure myograph (Danish Myo Tech, Model P100, J.P. Trading I/S, Aarhus, Denmark), as described (Briones *et al*., 2009). Briefly, vessels were placed in calcium-

free KHS ($0Ca^{2+}$; omitting calcium and adding 1 mM EGTA) and a pressure-diameter curve was obtained by increasing intraluminal pressure in 20 mmHg steps from 3 to 120 mmHg. Internal and external diameters were continuously measured under passive conditions (D_{i0Ca}, D_{e0Ca}) for 3 min at each intraluminal pressure. Finally, arteries were set to 45 mmHg in $0Ca^{2+}$-KHS and then pressure-fixed with 4% phosphate buffered PFA at 37°C for 60 min and kept at 4°C for confocal microscopy studies.

From internal and external diameter measurements in passive conditions the following structural and mechanical parameters were calculated:

$$\text{Wall thickness (WT)} = (D_{e0Ca} - D_{i0Ca})/2$$

$$\text{Wall:lumen} = (D_{e0Ca} - D_{i0Ca})/2D_{i0Ca}$$

Incremental distensibility represents the percentage of change in the arterial internal diameter for each mmHg change in intraluminal pressure, and was calculated according to the formula:

$$\text{Incremental distensibility} = \Delta D_{i0Ca}/(D_{i0Ca} \times \Delta P) \times 100$$

Circumferential wall strain (ε) = $(D_{i0Ca} - D_{00Ca})/D_{00Ca}$, where D_{00Ca} is the internal diameter at 3 mmHg and D_{i0Ca} is the observed internal diameter for a given intravascular pressure, both measured in $0Ca^{2+}$ medium.

Circumferential wall stress (σ) = $(P \times D_{i0Ca})/(2WT)$, where P is the intraluminal pressure (1 mmHg = 1.334×10^3 dynes·cm^{-2}) and WT is the wall thickness at each intraluminal pressure measured in $0Ca^{2+}$-KHS.

Arterial stiffness independent of geometry is determined by the Young's elastic modulus (E =stress/strain). The stress-strain relationship is non-linear; therefore, it is more appropriate to obtain a tangential or incremental elastic modulus (E_{inc}) by determining the slope of the stress-strain curve ($E_{inc}=\delta\sigma/\delta\varepsilon$). E_{inc} was obtained by fitting the stress-strain data from each animal to an exponential curve using the equation: $\sigma = \sigma_{orig} e^{\beta\varepsilon}$, where σ_{orig} is the stress at the original diameter (diameter at 3 mmHg). Taking derivatives on the equation presented earlier, we see that $E_{inc} = \beta\sigma$. An increase in β implies an increase in E_{inc}, which means an increase in stiffness.

Confocal microscopy study of nuclei distribution

Quantification of nuclei distribution was analyzed in pressure-fixed intact mesenteric segments, as described (Arribas *et al*., 1997). Briefly, arteries were incubated with the nuclear dye Hoechst 33342 (Sigma Chemical Co.) (0.01 mg·ml^{-1}) and visualized with a Leica TCS SP2 confocal system (Leica Microsystems, Wetzlar, Germany, ×40 objective, zoom ×3.5). Metamorph image analysis software (Universal Imaging, Molecular Devices Corp., Downingtown, PA, USA) was used for quantification.

To allow comparisons the following calculations were performed on the basis of 1-mm-long segments: artery volume (mm^3) [volume = wall CSA (mm^2) × 1 mm]; total number of adventitial and smooth muscle cells (cell n = n of nuclei per stack × n of stacks per artery volume); total number of endothelial cells [calculated per luminal surface of 1-mm-long artery; luminal surface area = 2π x diameter (mm) × 1 mm /2].

Organization of internal elastic lamina

The elastin organization within the internal elastic lamina (IEL) was studied in segments of small mesenteric arteries, using fluorescence confocal microscopy based on the autofluorescent properties of elastin (Ex 488 nm and Em 500-560 nm), as previously described (Briones *et al*., 2003). Briefly, intact pressure-fixed segments were visualized with a Leica TCS SP2 confocal system. From each stack of serial images, individual projections of the IEL were reconstructed, and total fenestrae number and fenestrae area were measured using Metamorph Image Analysis Software.

Collagen determination

Mesenteric arteries were cut into 5 μm sections using a cryostat. Collagen was quantified in Picro-sirius red-stained sections [0.1% (wt·vol^{-1}) Sirius red 3FB in saturated aqueous picric acid for 30 min with gentle agitation]. Three-four sections from each animal were analyzed under microscopy transmitted light (Leica DM 2000, Leica Microsystems) using an Image System Analysis (Leica LAS Image Analysis, Leica Microsystems). The area of collagen in the media layer was identified after excluding perivascular fibrosis of the vessel as the ratio of collagen deposition to the total media area.

Histological analysis

Cross sections (14 μm) from aortas were stained with hematoxylin-eosin. All images were acquired at room temperature using a microscope (Leica DM 2000). Morphometric determinations of the lumen and vessel areas were performed by using Metamorph Image Analysis Software. All microscopic images of the sections were traced for the calculations of the areas. To determine the luminal area, the cross-sectional area enclosed by the IEL was corrected to a circle by applying the form factor $l^2/4\pi$ to the measurement of the IEL, where l is the length of the lamina. Vessel area was determined by the cross-sectional area enclosed by the external elastic lamina corrected to a circle, applying the same form factor ($l^2/4\pi$) to the measurement of the external elastic lamina. The media area was calculated as the difference between the corrected vessel and luminal areas. Internal and external diameters were calculated from luminal and vessel areas, respectively. This method avoids miscalculations of areas caused by eventual collapse of the immersion-fixed arteries.

Vascular function

Reactivity of mice aorta was studied in a wire myograph. After a 30-min equilibration period in oxygenated KHS, arterial segments were stretched to their optimal lumen diameter for active tension development. Segments contractility was then tested by an initial exposure to a high-K^+ solution (K^+-KHS, 120 mM). The presence of endothelium was determined by the ability of 10 μM ACh to relax arteries precontracted with phenylephrine at approximately 50% the K^+-KHS contraction. Afterwards, a single concentration-response curve to ACh (1 nM-10 μM), phenylephrine (1 nM-10 μM) and diethylamine NONOate (DEA-NO, 3 nM-10 μM) was performed. The effects of the hydrogen peroxide detoxificant catalase (1000 U·ml^{-1}), the NAD(P)H oxidase inhibitor apocynin (0.3 mM), the selective NOX-1 inhibitor ML-171 (2-acetylphenothiazine, 0.5 μM), the mitochondrion-targeted SOD2 mimetic Mito-TEMPO (0.5 μM) or the non-selective inhibitor of NO synthesis, L-NAME (100 μM) on phenylephrine- or ACh-induced responses were analyzed. These drugs were incubated 30 min prior to phenylephrine.

Immunofluorescence

TLR4 in aorta was immunolocalized as described (de Batista *et al*., 2014). Briefly, frozen transverse sections (14 μm) were incubated with a polyclonal antibody against TLR4 (1:100, Santa Cruz Biotechnology Inc.) in PBS containing 2% bovine serum albumin for 1 h at 37ºC in a humidified chamber. After washing, rings were incubated with the secondary antibody goat anti-rat (1:200) IgG labelled with alexa fluor-546 dye (Molecular Probes Inc., Eugene, OR, USA), for 1 h at 37ºC in a humid box. Nuclei were stained with 0.01 mg·ml^{-1} Hoechst 33342. Immunofluorescent signals were viewed using an inverted Leica TCS SP2 confocal laser-scanning microscope with oil immersion lens. The specificity of the immunostaining was evaluated by omission of

the primary antibody and processed as above. Under these conditions, no staining was observed in the vessel wall.

Immunofluorescence was also used to detect p65 NF-κB subunit nuclear protein expression in cultured VSMC stimulated with AngII (100 nM, 45 min) after treatment or not with CLI-095 (1 μM, 1h), as described (Pérez-Girón *et al*., 2014). Cells were incubated overnight at 4°C with a rabbit polyclonal primary antibody against p65 (1:250, Santa Cruz Biotechnology). After washing, cells were incubated with a FITC-conjugated goat anti-rabbit secondary antibody (1:200, Molecular Probes, Life Technologies Ltd, Paisley, UK). Then, cells were counterstained for 15 min with DAPI (1:10,000, Invitrogen Life Technologies) and visualized under a fluorescence microscope (Zeiss, Axioplan 2, Carl Zeiss Microscopy, LLC, Thornwood, NY, USA). At least three independent experiments were performed.

Quantitative PCR real time (qRT-PCR) assay

mRNA levels were determined in mice aortic homogenates. Total RNA was obtained using TRI Reagent (Sigma Chemical Co.) according to the manufacturer's recommendations. A total of 1 μg of DNAse I treated RNA was reverse-transcribed using the High Capacity cDNA Archive Kit (Applied Biosystems, Foster City, CA, USA) in a final volume of 10 μl. qPCR was performed using the fluorescent dye SyBRGreen (iTaq FAST SyBRGreen Supermix with ROX, Bio-Rad, USA). β2-microglobulin (Rn00560865_m1, Applied Biosystems) or 36B4 were used as internal controls. All qPCRs were performed in duplicate. Primer sequences are: for TLR4, FW: TGTGCCTTCAAAACATGACTGG, RV: CTCCCAAGATCAACCGATGG; p22phox, FW: ATCTGTCTGCTGGAGTAT, RV: CGTAGTAATTCCTGGTGAG; NOX-1, FW: CAGCGTGCCGACAACAAG; RV: CCAGCCAGTGAGGAAGAGAC; TNF-α, FW: CCACGCTCTTCTGTCTACTG, RV: TGAGGGTCTGGGCCATAGA; MCP-1 (monocyte chemoattractant protein-1), FW: CATCCACGTGTTGGCTCA, RV: GATCATCTTGCTGGTGAATGAGT; IL-6, FW: TGATGGATGCTACCAAACTGG, RV: TTCATGTACTCCAGGTAGCTATGG; 36B4, FW: AGATGCAGCAGATCCGCAT, RV: GTTCTTGCCCATCAGCACC. qRT-PCR was carried out in an ABI PRISM 7000 Sequence Detection System (Applied Biosystems) using the following conditions: 2 min 50°C, 10 min 95°C and 40 cycles: 15 s 95ºC, 1 min 60ºC. At the end of the PCR, melting curve analysis was performed to show PCR product specificity. To calculate the relative index of gene expression, we employed the $2^{-\Delta\Delta Ct}$ method using untreated samples as calibrator.

Measurement of $O_2^{\cdot-}$ production

The oxidative fluorescent dye dihydroethidium (DHE) was used to evaluate production of $O_2^{\cdot-}$ *in situ*, as previously described (Martínez-Revelles *et al*., 2013). Briefly, aortic sections were incubated in buffer containing DHE (2 μM, 30 min, 37ºC) and then viewed by a fluorescent laser-scanning confocal microscope (Leica TCS SP2; Ex 561 and Em 610 nm), using the same imaging settings in each case. As a negative control, parallel sections were preincubated with tempol (100 μM). In these conditions, no staining was observed in the vascular wall. $O_2^{\cdot-}$ production was quantitatively analyzed with MetaMorph Image Analysis Software.

NAD(P)H oxidase activity

The lucigenin-enhanced chemiluminescence assay was used to determine the superoxide anion generated by NAD(P)H oxidase activity, as described (Pérez-Girón *et al*., 2014). Tissues were homogenized in a lysis buffer (in mM: KH_2PO_4 50, ethylene glycol tetraacetic acid 1, sucrose 150, pH=7.4). The reaction was started by the addition

of NAD(P)H (0.1 mM) to the suspension containing sample, lucigenin (5 μM), and assay phosphate buffer. The luminescence was measured in a plate luminometer (Auto-Lumat LB 953, Berthold Technologies GmbH & Co. KG, Bad Wildbad, Germany). Buffer blank was subtracted from each reading. Activity was expressed as relative light units·mg^{-1} protein. Samples from control+IgG-treated mice or untreated cells were used as controls, and variations of activity were calculated as the amount relative to controls.

Nitric oxide release

NO production was determined in aortic segments with the fluorescent probe 4,5-diaminofluorescein (DAF-2), as described (Martínez-Revelles *et al*., 2013). Briefly, aortic segments were incubated with DAF-2 (2 μM) for 45 min. Afterwards, basal and ACh-stimulated NO release were measured using a spectrofluorimeter (FLUOstar OPTIMA BMG Labtech). To avoid variations in fluorescence among the different days, all experimental conditions were measured each day. The amount of NO released was expressed as arbitrary units·mg^{-1} tissue.

Western blot analysis

Protein expression was determined in whole cell lysates (20 μg protein) or nuclear extracts (15 μg protein) by Western blot, as described. Proteins were separated by 15% SDS-PAGE and then transferred to polyvinyl difluoride membranes overnight. Membranes were incubated with rabbit polyclonal antibody for p-JNK1/2 (1:1,000, Cell Signaling Technology Inc, Danvers, MA, USA) or p65 (1:1,000). Immunoreactive bands were visualized using fluorescent secondary antibodies from rabbit (1:5,000, Bio-Rad, Laboratories, Hercules, CA, USA) and ECF Plus Western blot analysis system (GE Healthcare; Little Chalfont, UK). Signals on the immunoblot were quantified using the Typhoon 9210 quantification software (GE Healthcare). The same membrane was used to determine JNK (monoclonal antibody anti-JNK, 1:1,000, Cell Signaling Technology Inc) in cellular lysates and Histone-3 (rabbit polyclonal antibody anti-Histone-3, 1:500, Santa Cruz Biotechnology) in nuclear extracts. Results are expressed as the ratio between signals on the immunoblot corresponding to the different proteins and total JNK or Histone-3 in the same preparation. To compare results for protein expression within the same experiment and with others, we assigned a value of 1 in each gel to the expression of unstimulated control cells and used that value to calculate the relative density of other bands from the same gel.

Statistical analysis and drugs

Vasoconstrictor responses were expressed as a percentage of the tone generated by K^+-KHS. Vasodilator responses were expressed as the percentage of the previous tone induced by phenylephrine in each case. The maximum response (Emax) and pD_2 values were calculated by non-linear regression analysis of each individual concentration-response curve using GraphPad Prism Software (San Diego, CA, USA). To compare the effect of L-NAME on the response to phenylephrine in segments from the three groups, results were expressed as the differences of areas under the concentration-response curves (dAUC) in the control and experimental situations. AUCs were calculated from the individual concentration-response curve plots using GraphPad Prism Software; differences were expressed as the percentage of the AUC of the corresponding control situation.

All values are expressed as mean ± SEM of the number of animals or different cultures (each obtained from three different animals) used. Results were analyzed by using unpaired Student's *t*-test or two-way ANOVA followed by Bonferroni's post hoc

test or Mann-Whitney nonparametric test by using GraphPad Prism Software. A $P < 0.05$ was considered significant.

l-phenylephrine hydrochloride, ACh chloride, catalase, apocynin, L-NAME, and ML-171 were purchased from Sigma Chemical Co, mito-TEMPO from Santa Cruz Biotechnology Inc., DHE from Invitrogen, CLI-095 from Invivogen (San Diego, CA, USA) and ST-2825 from MedChem Express (Princeton, NJ, USA). All drugs were dissolved in distilled water, except for CLI-095 and ST-2825, which were dissolved in dimethyl sulfoxide (DMSO); 10 µl of DMSO did not have any effect on VSMC.

The receptor nomenclature conforms to BJP´s Concise Guide to Pharmacology according to Alexander *et al*. (2013).

Results

TLR4 mediates AngII-induced hypertension and inflammation

TLR4 mRNA levels were greater in aortic segments from AngII-infused mice when compared with controls (Figure 1A); TLR4 expression was increased in all layers of the vascular wall (Figure 1A).

Treatment with anti-TLR4 partially prevented the increased SBP observed in AngII-infused mice (Figure 1B), although neither body weight (data not shown) nor left ventricular hypertrophy were affected (Figure 1C).

Aortic segments from AngII-infused mice showed increased mRNA levels of TNFα, IL-6 and MCP-1 that were prevented by anti-TLR4 treatment (Figure 1D).

TLR4 mediates vascular remodelling and mechanical alterations

In small mesenteric arteries from AngII-infused mice, vessel and lumen diameters were reduced, while wall thickness and wall:lumen ratio were increased when compared with controls (Figure 2A-D). Treatment of AngII-infused mice with anti-TLR4 antibody improved these structural parameters (Figure 2A-D); the treatment also improved the reduced number of smooth muscle and endothelial cells observed in mesenteric arteries from AngII-infused mice (Figure 2E).

AngII infusion reduced incremental distensibility (Figure 3A) and increased vessel stiffness of mesenteric arteries, as shown by the leftward shift of the stress-strain relationship and the larger β value (Figure 3B) that were prevented by anti-TLR4 antibody treatment (Figure 3A,B). AngII reduced the number and size of fenestrae in the IEL (Figure 3C) and increased the collagen deposition (Figure 3D). Anti-TLR4 treatment improved fenestrae size and decreased collagen deposition (Figure 3C,D).

In aorta from AngII-infused mice, the media thickness, media:lumen ratio and cross-sectional area were increased when compared with controls; treatment with anti-TLR4 antibody prevented these structural alterations (Figure 4).

TLR4 mediates alterations on vascular function

Phenylephrine-induced contractile responses were greater in aortic segments from AngII-infused than control mice and these responses were reduced by anti-TLR4 antibody treatment (Figure 5A). Treatment also improved the reduced ACh-induced endothelium-dependent vasodilatation observed in aorta from AngII-infused mice (Figure 5B). Endothelium-independent relaxation induced by DEA-NO was similar in the three groups (Figure 5C).

TLR4 mediates vascular ROS production

The increased AngII-induced ROS production may contribute to the vascular alterations occurring in hypertension (Briones and Touyz, 2010; Virdis *et al*., 2011). As expected, $O_2^{\cdot-}$ production was greater in the aortic wall from AngII-infused than control mice; this was particularly evident in adventitia and media layers (Figure 6A). Aortic NAD(P)H oxidase activity (Figure 6B) and p22phox and NOX-1 mRNA levels (Figure 6C) were also greater in AngII-infused than control mice. Anti-TLR4 antibody treatment prevented the increased $O_2^{\cdot-}$ production, NAD(P)H oxidase activity and NOX-1 mRNA levels, without modifying p22phox levels (Figure 6).

We have previously described that AngII increases oxidative stress in VSMC through TLR4 activation (de Batista *et al*, 2014). Herein we observed that AngII (1 h)-induced NAD(P)H oxidase activity was reduced by the MyD88 inhibitor ST-2825 (Figure 7A). We have also reported that AngII increases oxidative stress in VSMC through JNK1/2 MAPK and NF-κB (Pérez-Girón *et al*., 2014). The AngII (10 min)-

induced JNK1/2 phosphorylation was reduced by the TLR4 inhibitor CLI-095 (Figure 7B). In addition, the increased nuclear expression and cytosol to the nucleus translocation of the p65 NF-κB subunit induced by AngII (45 min) was also reduced by CLI-095 (Figure 7C,D).

TLR4 mediates the contribution of oxidative stress to altered vascular function

We then assessed whether the increased ROS production associated with TLR4 upregulation contributes to the hypertension-associated vascular dysfunction. Catalase, apocynin, ML-171 and Mito-TEMPO did not affect phenylephrine-induced contraction in control mice, but they reduced those responses in AngII-infused mice; treatment of AngII-infused mice with the anti-TLR4 antibody abolished the inhibitory effect of the four antioxidants (Figure 8). Similarly, catalase, apocynin, ML-171 and Mito-TEMPO increased ACh-induced relaxation only in AngII-infused mice; anti-TLR4 antibody treatment abolished these effects (Figure 9). Altogether, these results suggest that TLR4 increased oxidative stress that would contribute to the impaired vascular function observed in hypertensive mice.

TLR4 reduces NO release and its participation in phenylephrine contraction

Thereafter, we evaluated the effects of the anti-TLR4 antibody treatment on the vascular NO release and its contribution to vasoconstrictor responses. In aorta from AngII-infused mice we observed a reduced NO release that was normalized by anti-TLR4 treatment (Figure 10A). Furthermore, the NOS inhibitor L-NAME leftward shifted the concentration-response curve to phenylephrine more in segments from control than AngII-infused mice; the anti-TLR4 antibody treatment restored this effect (Figure 10B and Table 1), indicating that the decreased NO involvement to phenylephrine contraction after AngII infusion is restored by TLR4 blockade.

Discussion

The results of the present study demonstrate, for the first time, that upregulation of TLR4 by AngII participates in the pathogenesis of hypertension by affecting, not only the function, but also the structure and the mechanical properties of the vasculature by mechanisms likely involving oxidative stress. MyD88-dependent mechanisms and the JNK/NF-κB signalling pathways might contribute to these effects.

Hypertension has been described as an inflammatory disease in which the inadequate activation of immune system may contribute to its pathophysiology (Savoia and Schiffrin, 2006; de Ciuceis *et al*., 2014; Harrison, 2014; McCarthy *et al*., 2014; Schiffrin, 2014; Virdis *et al*., 2014). The role of adaptive immunity as contributor of hypertension has been widely reported. Thus, subsets of T lymphocytes have been involved in the development of hypertension and vascular remodelling in different hypertension models (de Ciuceis *et al*., 2014; Harrison, 2014; Schiffrin, 2014; Virdis *et al*., 2014). Moreover, in the last years, activation of TLR4 has become a new research focus because of evidence that TLR4 is upregulated in hypertension contributing to its occurrence (Eiβler *et al*., 2011; Bomfin *et al*., 2012; de Batista *et al*., 2014; Sollinger *et al*., 2014). The increased expression of TLR4 by AngII is one of the proposed mechanisms explaining the involvement of this receptor in hypertension. Thus, AngII induces inflammatory responses via TLR4 activation. In this sense, in VSMC AngII, through AT1 receptors, activates TLR4 leading to ERK1/2 and NF-κB activation and hence inflammatory response (Ji *et al*., 2009); moreover, osteocalcin-induced AngII release activates PKCδ/TLR4/ROS/cyclooxygenase-2 signalling cascade that contributes to vascular fibroblasts transformation to myofibroblasts (Yuen *et al*., 2012). Recently we have shown that treatment with an AT1 receptor blocker reduced the increased TLR4 levels in SHR (de Batista *et al*., 2014). Herein we observed that AngII infusion increased aortic TLR4 expression. More importantly, anti-TLR4 antibody treatment prevented the increased blood pressure and vascular proinflammatory cytokine levels, confirming the role of TLR4 to the AngII-induced hypertension and the associated inflammation. In agreement, in SHR this treatment reduced blood pressure (Bomfim *et al*., 2012; de Batista *et al*., 2014) and the increased vascular proinflammatory cytokine levels (Bomfim *et al*., 2015). Further experiments are necessary to ascertain the exact mechanisms by which AngII upregulates TLR4 signalling pathway in our hypertension model.

The role of TLR4 in hypertension might rely on its effects on vascular structure and mechanical properties. TLR4 is involved in the outward arterial remodelling after atherosclerotic plaque formation (Hollestelle *et al*., 2004) and TLR through MyD88-dependent mechanisms contributes to the flow-mediated inward remodelling of conduit arteries (Tang *et al*., 2008). Furthermore, TLR4 gene Asp299Gly polymorphism is associated with increased carotid artery compliance in young adults (Hernesniemi *et al*., 2008). Our study provides evidence that TLR4 blockade prevents AngII-induced vascular remodelling and mechanical alterations, which might further contribute to the anti-hypertensive effects of the anti-TLR4 antibody treatment. Of note, these effects on vessel structure are observed in both conductance and resistance arteries, as demonstrated by the decreased wall:lumen ratio and wall thickness, which are well-known predictors of cardiovascular risk (Rizzoni and Agabiti-Rosei, 2012). Normalization of vessel structure by anti-TLR4 antibody treatment was achieved by improvement of cell number, which is reduced after AngII (Briones *et al*., 2009). Moreover, TLR4 blockade prevented the AngII-induced increased collagen deposition and altered elastin structure, probably accounting for the restored wall:lumen ratio and the diminished vessel stiffness observed in response to anti-TLR4 treatment.

Accordingly, in human VSMC the endogenous ligand for TLR4 HSP70 increases fibronectin and collagen type-I (González-Ramos *et al*., 2013). Besides improving vascular structure and mechanics, anti-TLR4 treatment normalized contractile responses and endothelial function in aortic segments from AngII-infused mice, in agreement with studies in SHR (Bomfin *et al*., 2012; de Batista *et al*., 2014). Moreover, we herein demonstrate that anti-TLR4 treatment also prevented the decreased endothelial cells number induced by AngII, thus providing a novel mechanism for endothelial improvement after TLR4 blockade.

One of the mechanism by which TLR4 blockade might prevent hypertension development and improve the vascular alterations found in AngII-infused mice is by reducing oxidative stress. Earlier studies described that antioxidants prevented hypertension development and structural alterations of both resistance and conductance arteries in AngII-infused mice (Virdis *et al*., 2004; Martínez-Revelles *et al*., 2013). The mechanisms responsible for the vascular alterations induced by increased ROS production include VSMC proliferation and migration, oxidation of matrix metalloproteinases and generation of matrix proteins such as collagen (Virdis *et al*., 2004; Briones *et al*., 2009; Drummond *et al*., 2011). Furthermore, the increase of ROS has been extensively reported to be responsible for endothelial dysfunction in hypertension (Briones and Touyz, 2010; Virdis *et al*., 2011). In addition, increased ROS production by TLR4 pathway contributes to the AngII effects on mesangial cells apoptosis and fibroblasts differentiation (Lv *et al*., 2009; Yuen *et al*., 2012). Herein, we found that anti-TLR4 antibody treatment reduced the increased NOX-1 expression, NAD(P)H oxidase activity and superoxide anion production observed in aorta from AngII-infused mice. Additionally, this treatment also abolished the effect of different antioxidants on both vasoconstrictor and vasodilator responses, confirming that TLR4 contributes to the endothelial dysfunction in AngII-induced hypertension by increasing oxidative stress, as suggested recently in other hypertension models (de Batista *et al*., 2014; Sollinger *et al*., 2014). Our results point to both NAD(P)H oxidase and mitochondria as sources for the TLR4-induced oxidative stress. As a result of oxidative stress reduction by anti-TLR4 antibody treatment, NO bioavailability might be increased. Thus, TLR4 blockade increases NO release and its contribution to the phenylephrine-induced vasoconstriction in AngII-infused mice. Accordingly, in obese and diabetic mice, TLR4 activation increases ROS levels leading to a reduced NO-production and bioavailability (Liang *et al*., 2013). The increased NO would also be related to the above mentioned increased number of endothelial cells. Altogether, our results suggest that oxidative stress reduction by TLR4 blockade might account for the beneficial effects not only on the functional but also on the structural and mechanical vascular alterations. Although the role of oxidative stress after TLR4 activation on vascular remodelling in hypertension has not been previously explored, superoxide-initiated inflammation is necessary for MyD88-dependent inward remodelling of conduit arteries induced by flow (Tang *et al*., 2008). Interestingly, TLR4 activation contributes to the vascular dysfunction associated with hypertension in SHR by cyclooxygenase-dependent mechanisms (Bomfim *et al*., 2012). Contractile prostanoids from COX-2 contribute to hypertension and also to the functional alterations observed in AngII-infused mice and this is in part dependent on ROS (Martínez-Revelles *et al*., 2013). Therefore, it is possible that by affecting oxidative stress status, TLR4 also modulates the COX pathway and its contribution to the vascular alterations associated with our hypertension model.

TLR4 signals through different adaptor proteins, mainly MyD88, ultimately activating NF-κB which promotes transcription of different proinflammatory genes

(Kawai and Akira, 2010). Another signalling pathway recruited by TLR4 activation via MyD88-dependent pathway is the MAPK cascade (Kawai and Akira, 2010). Previously we have shown that JNK and NF-κB contributes to the AngII-induced oxidative stress (Pérez-Girón *et al*., 2014). Herein we found, in VSMC, that AngII-induced NAD(P)H oxidase activity was reduced by a specific MyD88 inhibitor. Additionally, the TLR4 antagonist CLI-095 reduced the AngII-induced increased p65 nuclear expression and JNK1/2 phosphorylation. Altogether, our results suggest that after TLR4 upregulation, through the MyD88-dependent signalling pathway, AngII activates NF-κB/JNK, which would contribute to the increased oxidative stress and inflammation occurring in hypertension. Accordingly, Bonfim *et al*. (2015) have recently shown in SHR mesenteric arteries that TLR4 signalling is activated, leading to activation of MyD88/NF-κB pathway.

In conclusion, TLR4 upregulation by AngII contributes to the inflammation, endothelial dysfunction, vascular remodelling, extracellular matrix alterations and vascular stiffness associated with hypertension. These effects might be mediated by the MyD88/NF-κB/JNK pathways and increased oxidative stress from NAD(P)H oxidase and mitochondria. Although the role of adaptive immunity and T lymphocytes on vascular remodelling has been established (de Ciuceis *et al*., 2014; Harrison, 2014; Schiffrin, 2014; Virdis *et al*., 2014), to the best of our knowledge, this is the first time that the TLR4 signalling pathway is described to contribute to the vascular structural and mechanical alterations observed in hypertension. The fact that TLR is expressed not only in the immune but also in vascular cells allows to suggest that TLR4 might be the link between low-grade inflammation, vascular remodelling and hypertension. The current model is that in hypertension, the elevated circulating levels of several compounds which act as DAMPs, such as AngII, after being recognized by TLRs on antigen-presenting cells, would originate the activation of T cells; the release of cytokines and chemokines causes inflammation and subsequently vascular damage through several mechanisms, including oxidative stress. This results in increased blood pressure, leading to further damage which would increase the release of DAMPs, creating a positive feed-back loop which contributes to the maintenance of hypertension (de Ciuceis *et al*., 2014; Harrison, 2014; Schiffrin, 2014). Therefore, our observations open new antihypertensive therapeutic perspectives using agents that interfere with the TLR4 signalling pathway.

Acknowledgments

We are grateful to Dr. Ernesto Moro for his help in some experiments.

This work was supported by Ministerio de Economía y Competitividad (SAF2012-36400), Instituto de Salud Carlos III (Red de Investigación Cardiovascular RD12/0042/0024 and RD12/0042/0033) and URJC (PRIN13_CS12). AMB was supported by the Ramón y Cajal Program (RYC-2010-06473).

Conflicts of interest

None

References

Alexander SP, Benson HE, Faccenda E, Pawson AJ, Sharman JL, Spedding M *et al* (2013). The Concise Guide to PHARMACOLOGY 2013/14: catalytic receptors. Br J Pharmacol 170: 1676-1705.

Arribas SM, Hillier C, González C, McGrory S, Dominiczak AF, McGrath JC (1997). Cellular aspects of vascular remodeling in hypertension revealed by confocal microscopy. Hypertension 30: 1455-1464.

Bomfim GF, Dos Santos RA, Oliveira MA, Giachini FR, Akamine EH, Tostes RC *et al* (2012). Toll-like receptor 4 contributes to blood pressure regulation and vascular contraction in spontaneously hypertensive rats. Clin Sci 122: 535-543.

Bomfim GF, Echem C, Martins CB, Costa TJ, Sartoretto SM, Dos Santos RA *et al* (2015). Toll-like receptor 4 inhibition reduces vascular inflammation in spontaneously hypertensive rats. Life Sci 122: 1-7.

Briones AM, Arribas SM, Salaices M (2010). Role of extracellular matrix in vascular remodelling of hypertension. Curr Opin Nephrol Hypertens 19: 187-194.

Briones AM, González JM, Somoza B, Giraldo J, Daly CJ, Vila E *et al* (2003). Role of elastin in spontaneously hypertensive rat small mesenteric artery remodelling. J Physiol 552: 185-195.

Briones AM, Rodríguez-Criado N, Hernanz R, García-Redondo AB, Rodrigues-Díez RR, Alonso MJ *et al* (2009). Atorvastatin prevents angiotensin II-induced vascular remodeling and oxidative stress. Hypertension 54: 142-149.

Briones AM, Touyz RM (2010). Oxidative stress and hypertension: current concepts. Curr Hypertens Rep 12: 135-142.

Carpenter S, O'Neill LA (2009). Recent insights into the structure of Toll-like receptors and post-translational modifications of their associated signalling proteins. Biochem J 422(1): 1-10.

de Batista PR, Palacios R, Martín A, Hernanz R, Médici CT, Silva MASC *et al* (2014). Toll-Like Receptor 4 upregulation by angiotensin II contributes to hypertension and vascular dysfunction through reactive oxygen species production. PlosOne 9(8): e104020.

de Ciuceis C, Porteri E, Rizzoni D, Rizzardi N, Paiardi S, Boari GE *et al* (2007). Structural alterations of subcutaneous small-resistance arteries may predict major cardiovascular events in patients with hypertension. Am J Hypertens 20: 846-852.

de Ciuceis C, Rossini C, La Boria E, Porteri E, Petroboni B, Gavazzi A *et al* (2014). Immune mechanisms in hypertension. High Blood Press Cardiovasc Prev 21: 227-234.

den Dekker WK, Cheng C, Pasterkamp G, Duckers HJ (2010). Toll like receptor 4 in atherosclerosis and plaque destabilization. Atherosclerosis 209: 314-320.

Drummond GR, Selemidis S, Griendling KK, Sobey CG (2011). Combating oxidative stress in vascular disease: NADPH oxidases as therapeutic targets. Nat Rev Drug Discov 10: 453-471.

Eiβler R, Schmaderer C, Rusai K, Kühne L, Sollinger D, Lahmer T *et al* (2011). Hypertension augments cardiac Toll-like receptor 4 expression and activity. Hypertens Res 34: 551-558.

González-Ramos M, Calleros L, López-Ongil S, Raoch V, Griera M, Rodríguez-Puyol M *et al* (2013). HSP70 increases extracellular matrix production by human vascular smooth muscle through TGF-β1 up-regulation. Int J Biochem Cell Biol 45: 232-242.

Harrison DG (2014). The immune system in hypertension. Trans Am Clin Climatol Assoc 125: 130-138.

Hernesniemi JA, Raitakari OT, Kähönen M, Juonala M, Hutri-Kähönen N, Marniemi J *et al* (2008). Toll-like receptor 4 gene (Asp299Gly) polymorphism associates with carotid artery elasticity. The cardiovascular risk in young Finns study. Atherosclerosis 198: 152-159.

Hollestelle SC, De Vries MR, Van Keulen JK, Schoneveld AH, Vink A, Strijder CF *et al* (2004). Toll-like receptor 4 is involved in outward arterial remodeling. Circulation 109: 393-398.

Ji Y, Liu J, Wang Z, Liu N (2009). Angiotensin II induces inflammatory response partly via toll-like receptor 4-dependent signaling pathway in vascular smooth muscle cells. Cell Physiol Biochem 23: 265-276.

Jialal I, Kaur H, Devaraj S (2014). Toll-like receptor status in obesity and metabolic syndrome: a translational perspective. J Clin Endocrinol Metab 99: 39-48.

Kawai T, Akira S (2010). The role of pattern-recognition receptors in innate immunity: update on Toll-like receptors. Nat Immunol 11: 373-384.

Liang CF, Liu JT, Wang Y, Xu A, Vanhoutte PM (2013). Toll-like receptor 4 mutation protects obese mice against endothelial dysfunction by decreasing NADPH oxidase isoforms 1 and 4. Arterioscler Thromb Vasc Biol 33: 777-784.

Lv J, Jia R, Yang D, Zhu J, Ding G (2009). Candesartan attenuates Angiotensin II-induced mesangial cell apoptosis via TLR4/MyD88 pathway. Biochem Biophys Res Commun 380: 81-86.

Marketou ME, Kontaraki JE, Zacharis EA, Kochiadakis GE, Giaouzaki A, Chlouverakis G *et al* (2012). TLR2 and TLR4 gene expression in peripheral monocytes in nondiabetic hypertensive patients: the effect of intensive blood pressure-lowering. J Clin Hypertens (Greenwich) 14: 330-335.

Martín A, Pérez-Girón JV, Hernanz R, Palacios R, Briones AM, Fortuño A *et al* (2012). Peroxisome proliferator-activated receptor-γ activation reduces cyclooxygenase-2 expression in vascular smooth muscle cells from hypertensive rats by interfering with oxidative stress. J Hypertens 30: 315-326.

Martínez-Revelles S, Avendaño MS, García-Redondo AB, Alvarez Y, Aguado A, Pérez-Girón JV, *et al* (2013). Reciprocal relationship between reactive oxygen species and cyclooxygenase-2 and vascular dysfunction in hypertension. Antioxid Redox Signal 18: 51-65.

Mathiassen ON, Buus NH, Sihm I, Thybo NK, Mørn B, Schroeder AP *et al* (2007). Small artery structure is an independent predictor of cardiovascular events in essential hypertension. J Hypertens 25: 1021-1026.

McCarthy CG, Goulopoulou S, Wenceslau CF, Spitler K, Matsumoto T, Webb RC. (2014). Toll-like receptors and damage-associated molecular patterns: novel links between inflammation and hypertension. Am J Physiol Heart Circ Physiol 306: H184-H196.

Mulvany MJ (2008). Small artery remodelling in hypertension: causes, consequences and therapeutic implications. Med Biol Eng Comput 46: 461-467.

Münzel T, Sinning C, Post F, Warnholtz A, Schulz, E (2008). Pathophysiology, diagnosis and prognostic implications of endothelial dysfunction. Ann Med 40: 180-196.

Pérez-Girón JV, Palacios R, Martín A, Hernanz R, Aguado A, Martínez-Revelles S *et al* (2014). Pioglitazone reduces angiotensin II-induced COX-2 expression through inhibition of ROS production and ET-1 transcription in vascular cells from spontaneously hypertensive rats. Am J Physiol Heart Circ Physiol 306: H1582-H1593.

Ponticos M, Smith BD (2014). Extracellular matrix synthesis in vascular disease: hypertension, and atherosclerosis. J Biomed Res 28: 25-39.

Rizzoni D, Agabiti-Rosei E (2012). Structural abnormalities of small resistance arteries in essential hypertension. Intern Emerg Med 7: 205-212.

Savoia C, Schiffrin EL (2006). Inflammation in hypertension. Curr Opin Nephrol Hypertens 15: 152-158.

Schiffrin EL (2014). Immune mechanisms in hypertension and vascular injury. Clin Sci 126: 267-274.

Sollinger D, Eiβler R, Lorenz S, Strand S, Chmielewski S, Aoqui C *et al* (2014). Damage-associated molecular pattern activated Toll-like receptor 4 signalling modulates blood pressure in L-NAME-induced hypertension. Cardiovasc Res 101: 464-472.

Tang PC, Qin L, Zielonka J, Zhou J, Matte-Martone C, Bergaya S *et al* (2008). MyD88-dependent, superoxide-initiated inflammation is necessary for flow-mediated inward remodeling of conduit arteries. J Exp Med 205: 3159-3171.

Touyz RM (2005). Intracellular mechanisms involved in vascular remodelling of resistance arteries in hypertension: role of angiotensin II. Exp Physiol 90: 449-455.

Tsan MF, Gao B (2004). Endogenous ligands of Toll-like receptors. J Leukoc Biol 76: 514-519.

Virdis A, Dell'Agnello U, Taddei S (2014). Impact of inflammation on vascular disease in hypertension. Maturitas 78: 179-183.

Virdis A, Duranti E, Taddei S (2011). Oxidative stress and vascular damage in hypertension: role of angiotensin II. Int J Hypertens 2011, 916310.

Virdis A, Neves MF, Amiri F, Touyz RM, Schiffrin EL (2004). Role of NAD(P)H oxidase on vascular alterations in angiotensin II-infused mice. J Hypertens 22: 535-542.

Wolf G, Bohlender J, Bondeva T, Roger T, Thaiss F, Wenzel UO (2006). Angiotensin II upregulates toll-like receptor 4 on mesangial cells. J Am Soc Nephrol 17: 1585-1593.

Yuen CY, Wong SL, Lau CW, Tsang SY, Xu A, Zhu Z *et al* (2012). From skeleton to cytoskeleton: osteocalcin transforms vascular fibroblasts to myofibroblasts via angiotensin II and Toll-like receptor 4. Circ Res 111: e55-66.

Figure legends

Figure 1. Increased TLR4 contributes to hypertension and inflammation in AngII-infused mice. (A) TLR4 mRNA levels and representative fluorescent confocal photomicrographs (×40 objective) of TLR4 immunolocalization in aortic segments from mice treated with a non-specific IgG and from mice treated with AngII plus a non-specific IgG. Image size: 375 x 375 µm. Positive immunostaining is indicated by arrows and the insets are magnified images of indicated areas. (B) Systolic BP (SBP), (C) left ventricular hypertrophy and (D) mRNA levels of MCP-1, IL-6 and TNFα in mice treated with a non-specific IgG, with AngII plus a non-specific IgG or with AngII plus anti-TLR4 antibody. *$P < 0.05$ *vs* Control + IgG, $^{\#}P < 0.05$ *vs* AngII + IgG. n=6-16.

Figure 2. **TLR4 inhibition improves structural alterations in mesenteric resistance arteries from AngII-infused mice.** Vessel and lumen diameter (A,B), wall thickness (C), wall:lumen ratio (D) and total number of adventitial, smooth muscle and endothelial cells (E) in small mesenteric arteries from mice treated with a non-specific IgG, with AngII plus a non-specific IgG or with AngII plus anti-TLR4 antibody. *$P <$ 0.05 *vs* Control + IgG, $^{\#}P < 0.05$ *vs* AngII + IgG. n=6-14.

Figure 3. TLR4 inhibition improves mechanical alterations in mesenteric resistance arteries from AngII-infused mice. Incremental distensibility (A) and stress-strain relationship and β values (B) in mesenteric arteries from mice treated with a non-specific IgG, with AngII plus a non-specific IgG or with AngII plus anti-TLR4 antibody. (C) Representative confocal projections and quantification of fenestra area and total number of fenestra of the internal elastic lamina of mesenteric arteries from the three groups of mice. Projections were obtained from serial optical sections captured with a fluorescence confocal microscope (×40 objective, zoom ×7.10); image size: 52.8 x 52.8 µm. (D) Representative images and quantitative analysis of collagen content in the media layer from transversal sections of mesenteric arteries. Images were captured with a light microscope (×40 objective); image size: 310.9 x 233.1 µm. *$P < 0.05$ *vs* Control + IgG, $^{\#}P < 0.05$ *vs* AngII + IgG. n=6-14.

Figure 4. TLR4 inhibition improves structural alterations in aorta from AngII-infused mice. (A) Representative photographs of hematoxylin-eosin aortic sections from mice treated with a non-specific IgG, with AngII plus a non-specific IgG or with AngII plus anti-TLR4 antibody. Images were captured with a light microscope (×10 objective); image size: 2.37 x 1.88 mm. (B) Media thickness, (C) media:lumen ratio and (D) cross-sectional area (CSA) in aorta from the three groups of mice. **P* < 0.05 *vs* Control + IgG, $^{\#}P < 0.05$ *vs* AngII + IgG. *n*=7-8.

Figure 5. TLR4 inhibition improves vasoconstrictor and vasodilator responses in aorta from AngII-infused mice. Concentration-response curves to phenylephrine (Phe) (A), ACh (B) and diethylamine NONOate (DEA-NO) (C) in aorta from mice treated with a non-specific IgG, with AngII plus a non-specific IgG or with AngII plus anti-TLR4 antibody. *$P < 0.05$ *vs* Control + IgG, $^{\#}P < 0.05$ *vs* AngII + IgG. n=12-17.

Figure 6. TLR4 inhibition reduces the increased oxidative stress in aorta from AngII-infused mice. (A) Representative fluorescent confocal photomicrographs and quantification in the media and in the adventitia of vascular superoxide anion production in aortic segments from mice treated with a non-specific IgG, with AngII plus a non-specific IgG or with AngII plus anti-TLR4 antibody. Vessels were labelled with the oxidative dye dihydroethidium and view by using a fluorescence confocal microscope (×40 objective). Image size 375 x 375 µm. (B) Basal NAD(P)H oxidase activity and (C) NOX-1 and p22phox mRNA levels in aorta from the three groups of mice. *$P < 0.05$ *vs* Control + IgG, $^{\#}P < 0.05$ *vs* AngII + IgG. n=5-8.

Figure 7. AngII activates Myd88, JNK and NF-κB in vascular smooth muscle cells (VSMC). (A) Effect of ST-2825 (20 μM, 1 h) on AngII (100 nM, 1 h)-induced NADPH oxidase activity. (B) Effect of CLI-095 (1 μM, 1 h) on AngII (10 min)-induced p-JNK1/2 protein expression; a representative blot is shown above. (C) Effect of CLI-095 on nuclear p65 NF-κB protein expression induced by AngII (45 min); representative blots of the cytosolic (Cy) and nuclear (Nu) expression are shown above; Histone-3 (H3) expressions are also shown to guarantee the successful cellular fractioning. (D) Representative photomicrographs of p65 NF-κB immunofluorescence (red) in VSMC in control and after incubation with AngII in the absence and the presence of CLI-095. The insets are magnified images of indicated areas. Images were captured with a fluorescence microscope (×20 objective); image size: 444.16 x 332.8 μm. *$P < 0.05$ *vs.* Control, $^{\#}P < 0.05$ *vs.* AngII. n=4-5.

Figure 8. TLR4 inhibition reduces the involvement of oxidative stress on vasoconstrictor responses in aorta from AngII-infused mice. Effect of catalase (1000 $U \cdot ml^{-1}$), apocynin (0.3 mM), ML-171 (0.5 μM) and Mito-TEMPO (0.5 μM) on the concentration-response curve to phenylephrine (Phe) in aortic segments from mice treated with a non-specific IgG, with AngII plus a non-specific IgG or with AngII plus anti-TLR4 antibody. $*P < 0.05$. n=5-11.

Figure 9. TLR4 inhibition reduces the involvement of oxidative stress on vasodilator responses in aorta from AngII-infused mice. Effect of catalase (1000 $U \cdot ml^{-1}$), apocynin (0.3 mM), ML-171 (0.5 μM) and Mito-TEMPO (0.5 μM) on the concentration-response curve to ACh in aortic segments from mice treated with a non-specific IgG, with AngII plus a non-specific IgG or with AngII plus anti-TLR4 antibody. * $P < 0.05$. n=5-11.

Figure 10. TLR4 inhibition increases NO production and its participation on vasoconstrictor responses in AngII-infused mice. (A) Quantification of NO release in aortic segments from mice treated with a non-specific IgG, with AngII plus a non-specific IgG or with AngII plus anti-TLR4 antibody. (B) Effect of N^G-nitro-L-arginine methyl ester (L-NAME, 100 μM) on the concentration-response curve to phenylephrine (Phe) in aortic segments from the three groups of mice. Differences of the area under the concentration-response curve (dAUC) to Phe in the presence and the absence of L-NAME are also shown. $^*P < 0.05$ *vs* Control or *vs* Control + IgG, $^{\#}P < 0.05$ *vs* AngII + IgG. *n*=5-9.

Table 1 Effect of L-NAME on maximum response (Emax) and pD_2 values of phenylephrine responses in aortic segments from mice treated with a non-specific IgG, with AngII plus a non-specific IgG or with AngII plus anti-TLR4 antibody.

		Control	L-NAME	Fold increase
Control + IgG	**Emax (%)**	30.1 + 2.6	85.7 + 6.4*	2.84 + 0.21
	pD_2	6.53 + 0.17	7.12 + 0.06*	-
AngII + IgG	**Emax (%)**	89.6 + 4.2$^{\#}$	148.2 + 17.7*$^{\#}$	1.65 + 0.20$^{\#}$
	pD_2	7.02 + 0.04$^{\#}$	7.30 + 0.07*	-
AngII + anti-TLR4	**Emax (%)**	44.8 + 8.7$^{\$}$	103.7 + 9.8*$^{\$}$	2.32 + 0.22$^{\$}$
	pD_2	6.72 + 0.08$^{\$}$	7.02 + 0.07*$^{\$}$	-

The enhancing effect of L-NAME in Emax is expressed as fold increase over control situation.*$P < 0.05$ vs Control; $^{\#}P < 0.05$ vs Control + IgG mice; $^{\$}P < 0.05$ vs Ang + IgG mice; n=5-9.

Formatted Table

Alonso_fig1

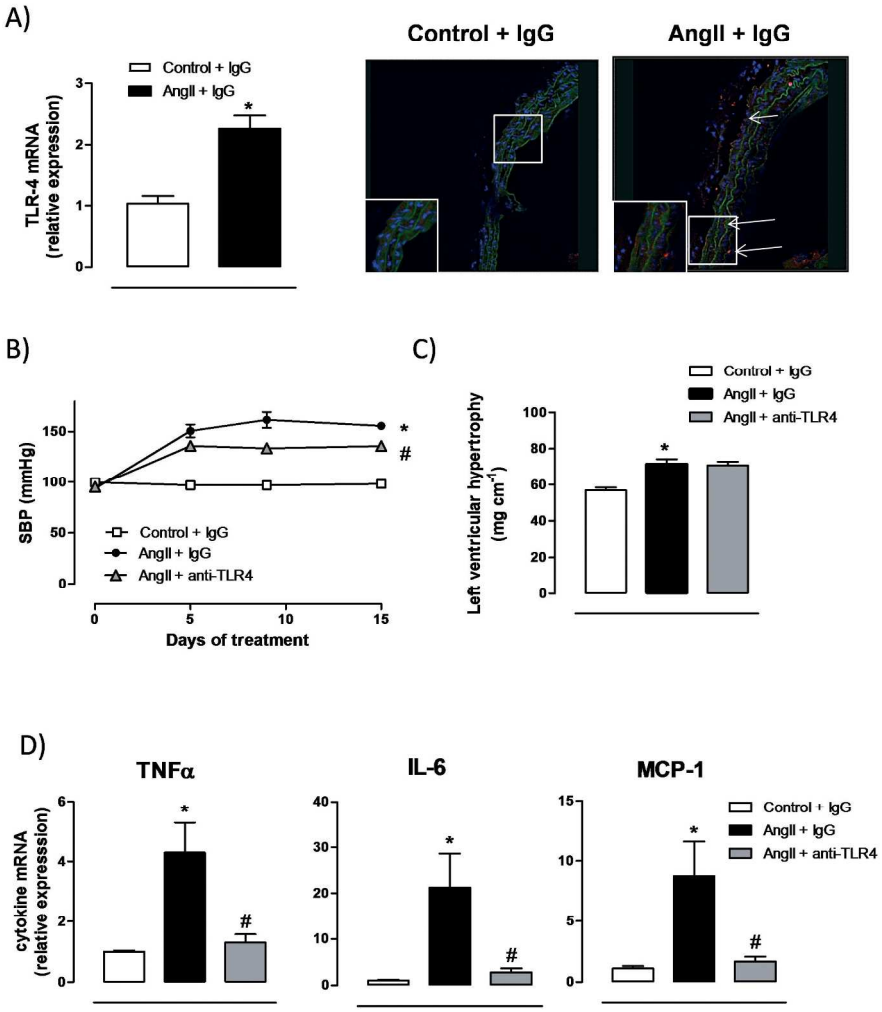

254x338mm (300 x 300 DPI)

Alonso_fig2

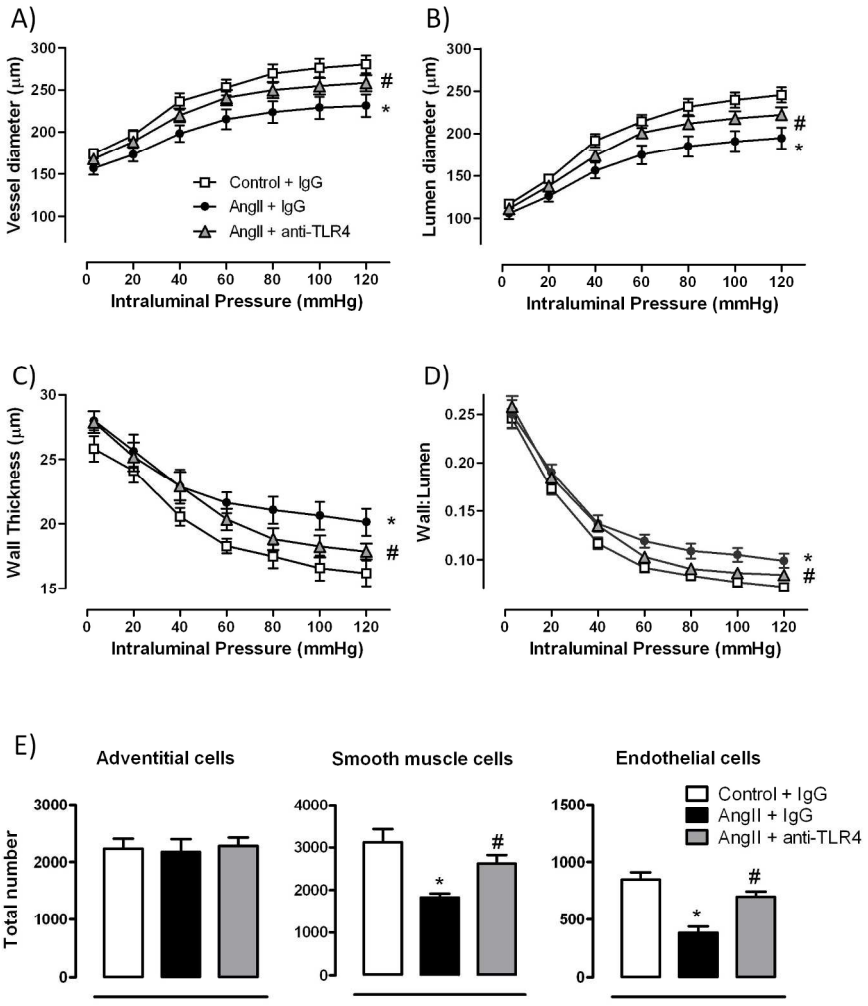

254x338mm (300 x 300 DPI)

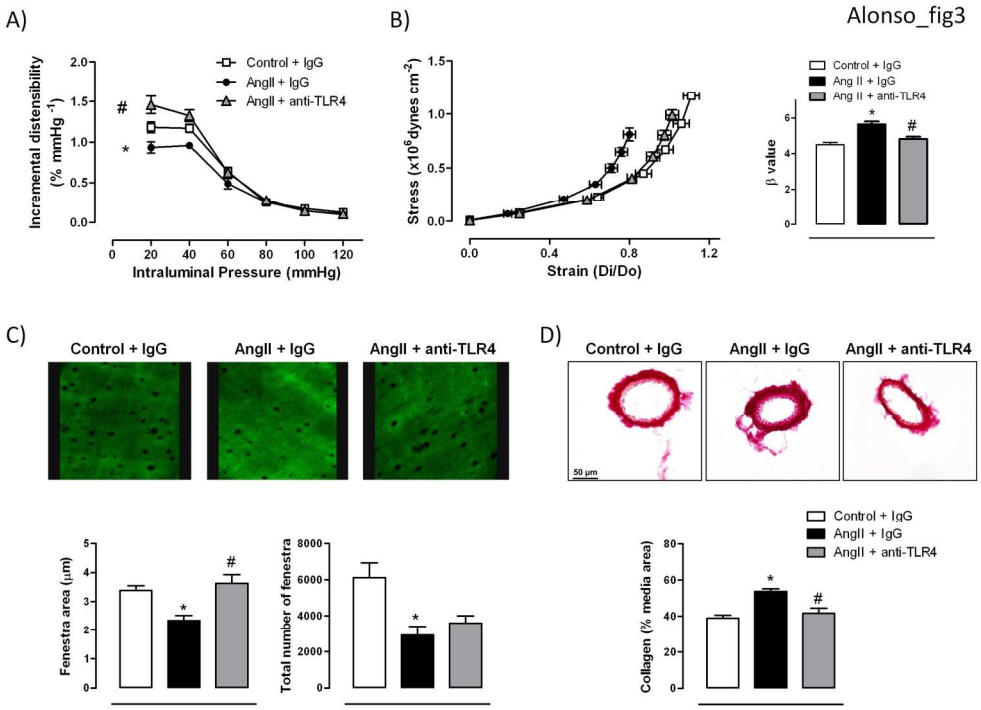

190x142mm (300 x 300 DPI)

Alonso_fig4

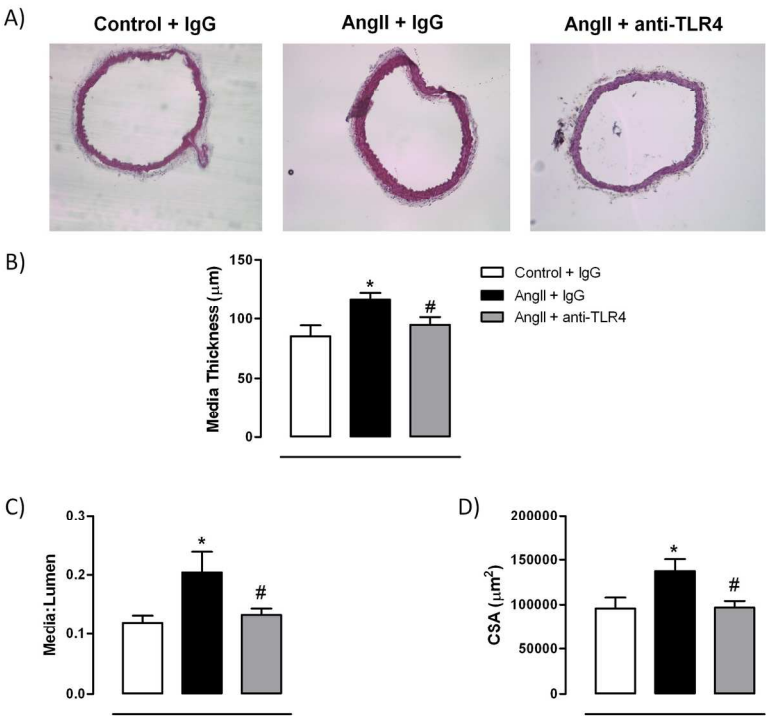

190x142mm (300 x 300 DPI)

Alonso_fig5

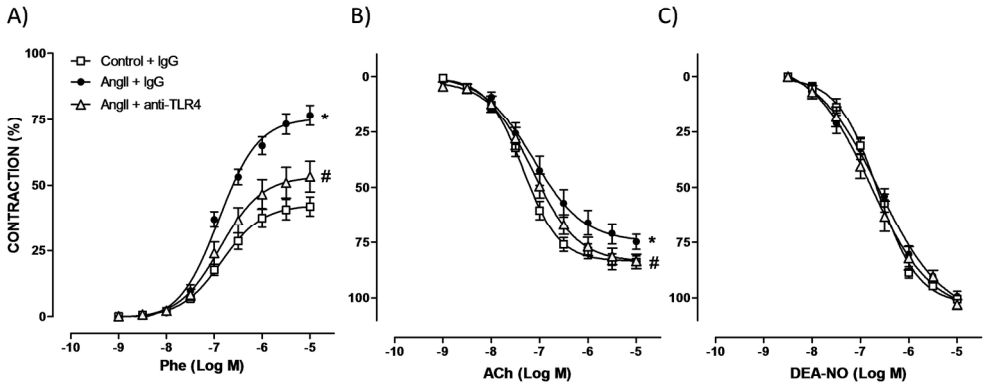

190x142mm (300 x 300 DPI)

Alonso_fig6

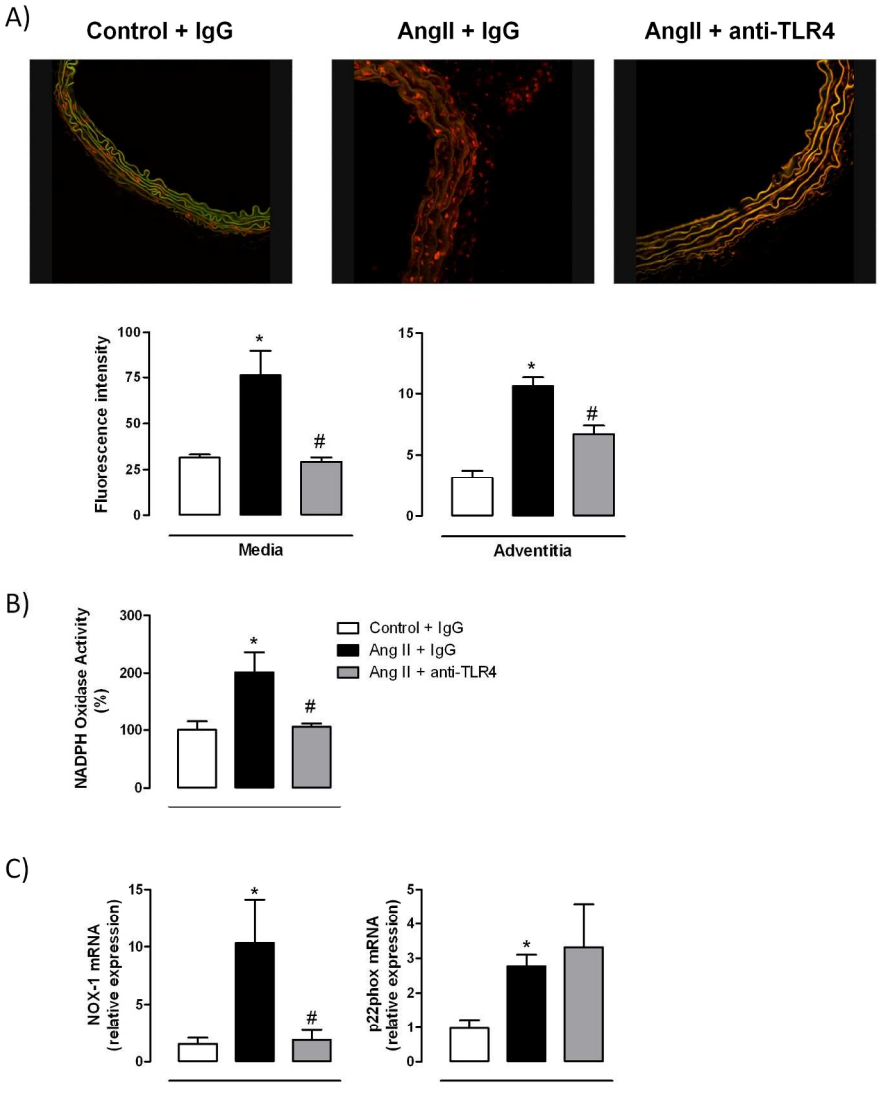

254x338mm (300 x 300 DPI)

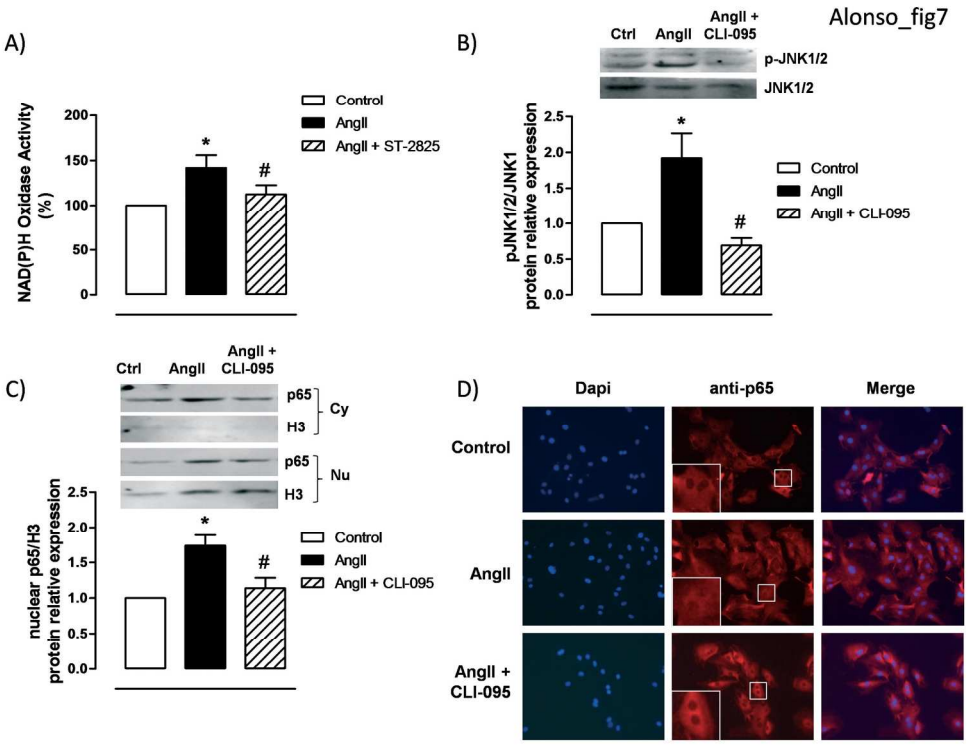

190x142mm (300 x 300 DPI)

Alonso_fig8

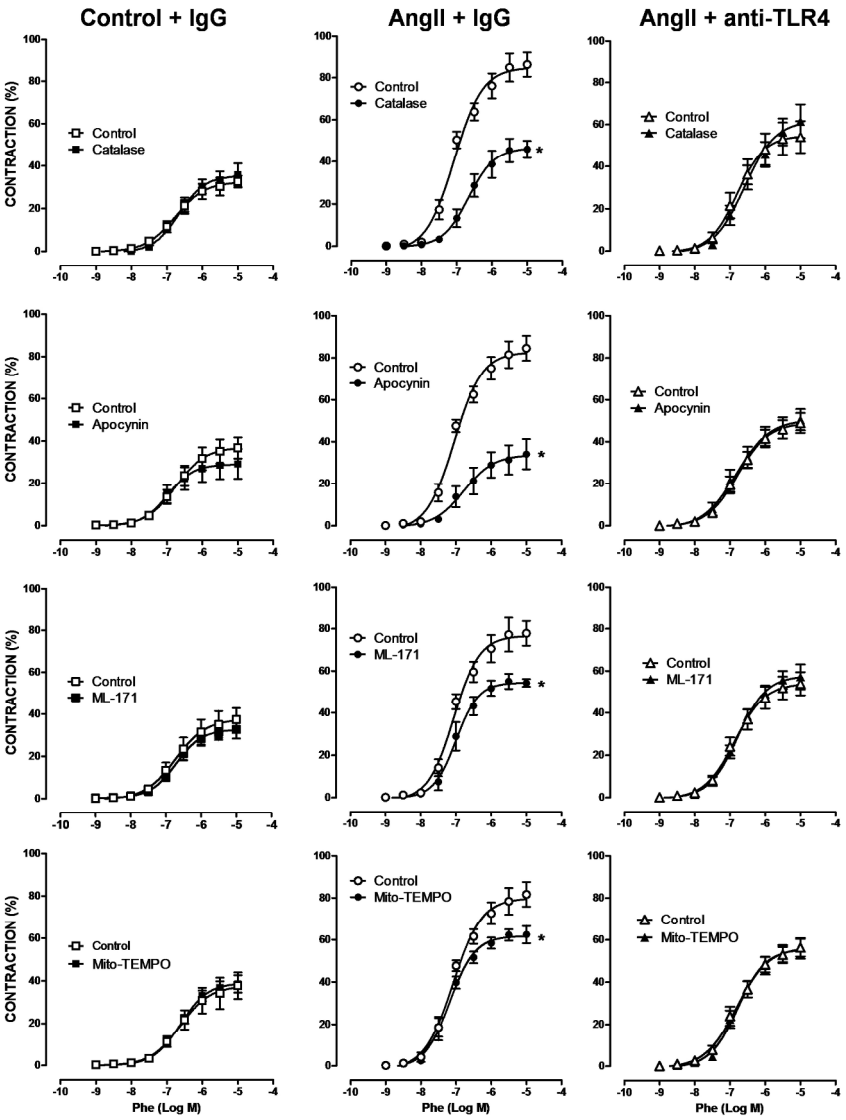

254x338mm (300 x 300 DPI)

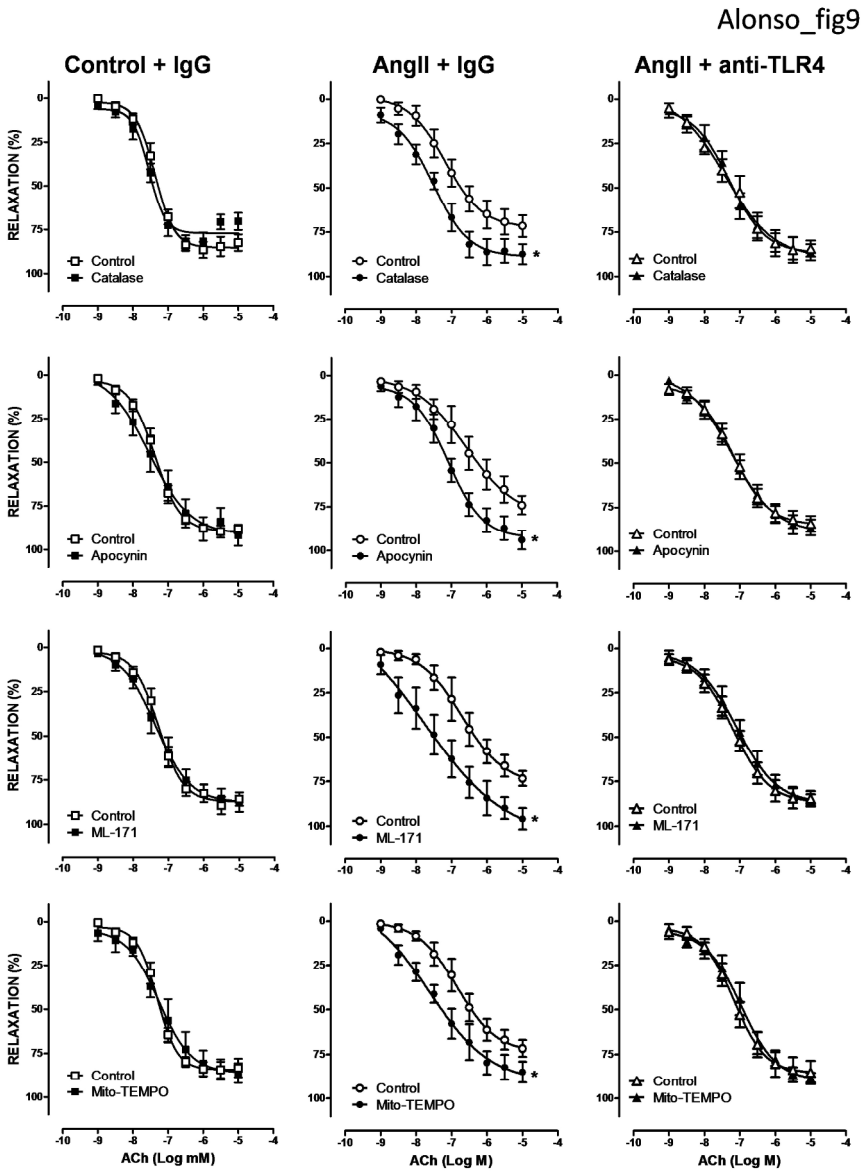

254x338mm (300 x 300 DPI)

Alonso_fig10

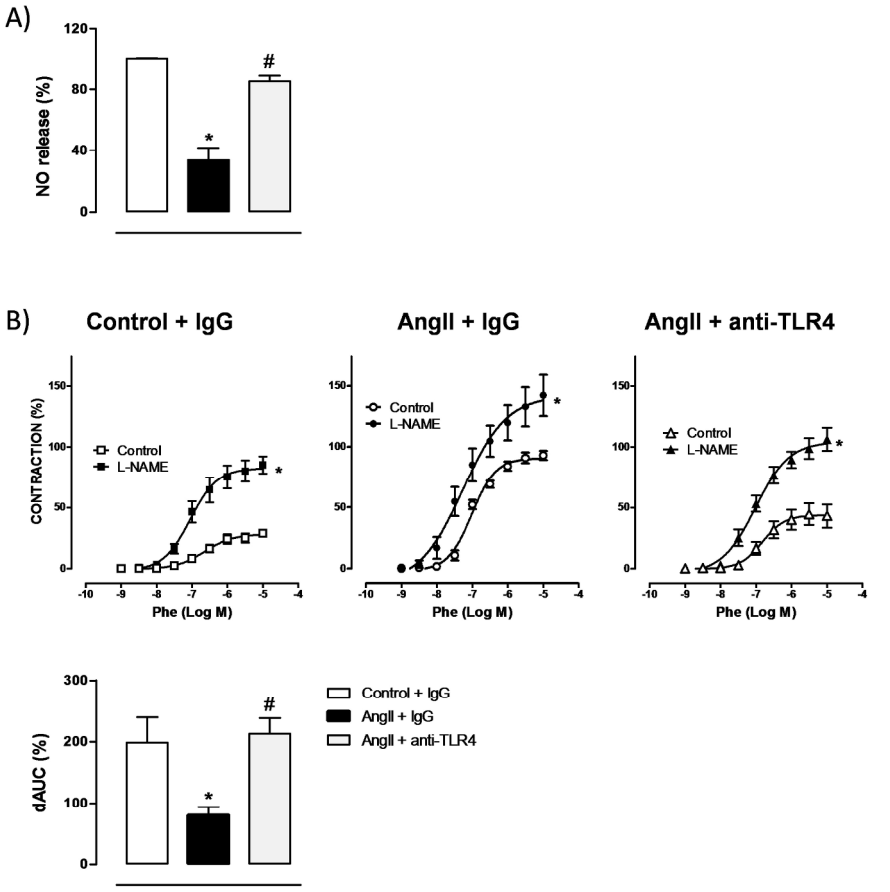

254x338mm (300 x 300 DPI)